Rapid Communications

Stabilizing two-dimensional quantum scars by deformation and synchronization

A. A. Michailidis,[1] C. J. Turner,[2] Z. Papić,[2] D. A. Abanin,[3] and M. Serbyn[1]
[1]*IST Austria, Am Campus 1, 3400 Klosterneuburg, Austria*
[2]*School of Physics and Astronomy, University of Leeds, Leeds LS2 9JT, United Kingdom*
[3]*Department of Theoretical Physics, University of Geneva, 24 quai Ernest-Ansermet, 1211 Geneva, Switzerland*

(Received 13 March 2020; accepted 27 April 2020; published 22 June 2020)

Relaxation to a thermal state is the inevitable fate of nonequilibrium interacting quantum systems without special conservation laws. While thermalization in one-dimensional systems can often be suppressed by integrability mechanisms, in two spatial dimensions thermalization is expected to be far more effective due to the increased phase space. In this work we propose a general framework for escaping or delaying the emergence of the thermal state in two-dimensional arrays of Rydberg atoms via the mechanism of quantum scars, i.e., initial states that fail to thermalize. The suppression of thermalization is achieved in two complementary ways: by adding local perturbations or by adjusting the driving Rabi frequency according to the local connectivity of the lattice. We demonstrate that these mechanisms allow us to realize robust quantum scars in various two-dimensional lattices, including decorated lattices with nonconstant connectivity. In particular, we show that a small decrease of the Rabi frequency at the corners of the lattice is crucial for mitigating the strong boundary effects in two-dimensional systems. Our results identify synchronization as an important tool for future experiments on two-dimensional quantum scars.

DOI: 10.1103/PhysRevResearch.2.022065

I. INTRODUCTION

Recent experimental breakthroughs allow us to probe nonequilibrium quantum dynamics of various isolated quantum systems [1–3]. Yet, for generic interacting systems that do not have any special conservation laws, such dynamics lead to a thermal state. This process of thermalization is explained by the typicality of highly excited eigenstates in interacting quantum systems. Formally, the eigenstate thermalization hypothesis (ETH) [4,5] conjectures that all eigenstates of a Hamiltonian in a sufficiently narrow energy shell display the same expectation values of physical observables as the microcanonical ensemble. ETH has been numerically and experimentally verified in a variety of different quantum systems [6,7].

To observe long-time coherent dynamics in quantum systems one must avoid thermalization or at least delay its onset. Integrable systems which satisfy the Yang-Baxter equation [8,9], and the disordered systems which undergo a many-body localization (MBL) transition [10,11], provide explicit examples of ETH violation. However, integrability is known to exist only for one-dimensional (1D) systems; the existence of MBL in higher dimensions is also debated [12,13]. Intuitively, thermalization is more ubiquitous in higher dimensions due to larger phase space available for relaxation processes. This motivates the exploration of alternative ETH-violating mechanisms.

Recent experiments on Rydberg atom arrays [14] suggested the possibility of *weak* ETH breaking via a different mechanism now known as "quantum many-body scars" [15,16]. Quantum many-body scarring manifests itself as the presence of a small set of atypical ETH-breaking eigenstates. Experimentally, scars lead to strong dependence of relaxation on initial conditions: initial configurations that have a large overlap with atypical eigenstates feature slow growth of entanglement and long-time coherent dynamics, whereas other initial states relax much faster. Theoretically, scars have been explained via the existence of an (un)stable trajectory within the variational semiclassical approach [16,17] or, alternatively, via a hidden su(2) algebra representation in the subspace of atypical eigenstates [18,19]. In addition, some exact scarred eigenstates of the Rydberg atom chain have been constructed [20], and their stability under perturbations was investigated [21,22]. Finally, scars were also reported in a variety of other models [23–35], while scarring may be related to nonergodic behavior observed in models with confinement [36–39], dynamical symmetries [40,41], fractons [42–44], and "Krylov restricted thermalization" [45].

In this work we present a detailed study of scars on two-dimensional (2D) lattices of Rydberg atoms in the regime of the nearest-neighbor blockade that has been realized in many recent experiments [3,14,46,47]. We concentrate on experimental knobs that could be used to enhance many-body scars in 2D quantum systems, which are significantly more susceptible to thermalization as well as finite-size effects due to their larger boundary-to-bulk ratio. First, we show that weak perturbations of the Rydberg atom Hamiltonian on square lattices can significantly stabilize scars by improving

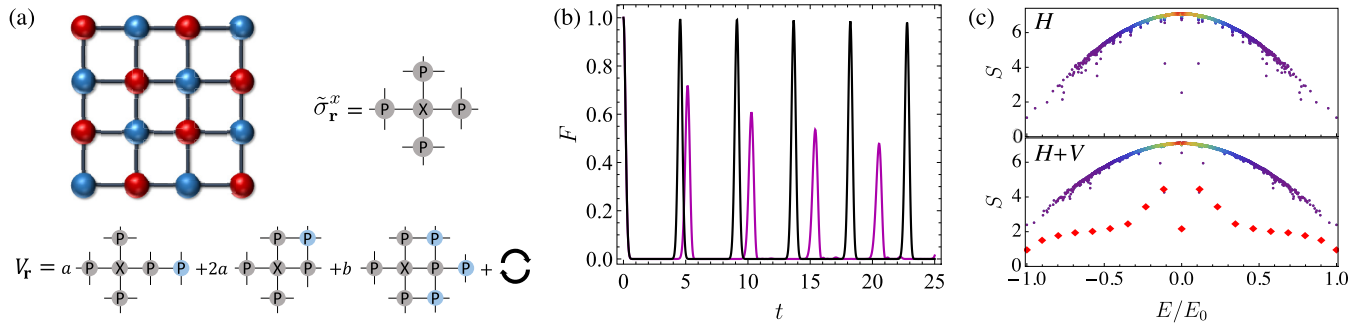

FIG. 1. (a) Square lattice, Hamiltonian density operator, Eq. (1), and the deformation, Eq. (2), needed to stabilize the scars. (b) Fidelity of quantum many-body revivals for the unperturbed Hamiltonian (magenta) and the model with the optimal perturbation (black) for a 6×6 lattice with PBC. (c) Entanglement entropy for all eigenstates as a function of their energy. The color indicates the density of dots, which is strongly peaked around zero energy. The deformed model (bottom plot) has a much more pronounced band of low-entangled eigenstates (red diamonds) compared with the undeformed model (top plot). Data are obtained by exact diagonalization in the zero-momentum, inversion-symmetric sector for the 6×6 lattice with $\mathrm{Dim}(\mathcal{H}) = 9702$ states.

an approximate su(2) algebra representation in the subspace of scarred eigenstates. This leads to stronger fidelity revivals and enhanced coherence in the dynamics. Furthermore, we consider scars on more complicated lattices and in the presence of open boundaries. For lattices featuring nonuniform connectivity, coherent many-body oscillations can be stabilized by adjusting the driving Rabi frequency according to local connectivity. We refer to this stabilization mechanism as "enforced synchronization," and we demonstrate that this can be used to suppress the dephasing due to the boundary by matching the oscillation frequency at the boundary and in the bulk.

II. MODEL

We begin by considering Rydberg atoms arranged in a square lattice in the regime of the nearest-neighbor blockade. The Hamiltonian generates Rabi oscillations of a given atom under the constraint that all four neighboring atoms are in the ground state,

$$H = \sum_{\mathbf{r}} \sigma^x_{\mathbf{r}} \prod_{\langle \mathbf{r}', \mathbf{r} \rangle} P_{\mathbf{r}'} = \sum_{\mathbf{r}} \tilde{\sigma}^x_{\mathbf{r}}, \tag{1}$$

where the indices $\mathbf{r} = (i, j)$ denote the lattice site, $i, j = 1, \ldots, L$, and the product goes over all nearest neighbors of site $\mathbf{r}$. The operator $\sigma^x_{\mathbf{r}} = |\uparrow\rangle\langle\downarrow| + |\downarrow\rangle\langle\uparrow|$ describes Rabi oscillations between excited ($\uparrow$) and ground states ($\downarrow$) of a given atom. The product of projectors onto the ground state, $P = |\downarrow\rangle\langle\downarrow|$, ensures the absence of excitations on nearest-neighbor sites. In Fig. 1(a) we show the lattice and the corresponding Hamiltonian density operator $\tilde{\sigma}^x_{\mathbf{r}}$. We focus on the sector of the Hilbert space with no adjacent excitations, which is the largest sector of the system. The dimension of this sector scales as $\mathrm{Dim}(\mathcal{H}) \propto c_1^{L^2}$ where $c_1 \approx 1.503\ldots$ is the hard square entropy constant [48].

III. STABILIZATION OF SCARS VIA DEFORMATION

Figure 1(a) shows a partition of the square lattice $\mathcal{M}$ into two sublattices, $\mathcal{M} = A \cup B$. Two states with the maximum number of excitations (compatible with the constraint of no adjacent excitations), $|M_A\rangle$ ($|M_B\rangle$), correspond to all the atoms in sublattice A (B) being in the excited state. In Ref. [17], it was shown that the fidelity, $F(t) = |\langle M_A|e^{-iHt}|M_A\rangle|^2$, which quantifies a probability of returning to the many-body state $|M_A\rangle$ at time t features persistent revivals with period T. These revivals were attributed to the existence of a periodic trajectory in the variational manifold of tree tensor states.

Figure 1(b) shows the revivals for a 6×6 square lattice with periodic boundary conditions (PBCs). The persisting oscillations of fidelity have a period of $T \approx 5$, where at half period the system is approximately close to the second maximally excited state $|M_B\rangle$. This dynamics is similar to the 1D case where the system oscillates between the two Neél states [14]. The revivals are decaying, and it is interesting to find small deformations that would enhance them.

To improve the revival quality, we propose the following deformation of the Hamiltonian, see Fig. 1(a):

$$V = \sum_{\mathbf{r}} V_{\mathbf{r}}, \quad V_{\mathbf{r}} = \tilde{\sigma}^x_{\mathbf{r}} \left(a\mathcal{P}^l_{\mathbf{r}} + 2a\mathcal{P}^d_{\mathbf{r}} + b\mathcal{P}^3_{\mathbf{r}} \right), \tag{2}$$

where a and b are parameters to be optimized and the projectors are defined as

$$\mathcal{P}^l_{i,j} = P_{i,j+2} + \cdots, \tag{3a}$$

$$\mathcal{P}^d_{i,j} = P_{i+1,j+1} + \cdots, \tag{3b}$$

$$\mathcal{P}^3_{i,j} = P_{i-1,j+1} P_{i,j+2} P_{i+1,j+1} + \cdots. \tag{3c}$$

Ellipses in Eqs. (3) denote the three remaining terms obtained by 90° rotations around the lattice site at position $\mathbf{r} = (i, j)$ that make the perturbation invariant under the full space group symmetry. Our heuristics on the choice of perturbations are based on the "forward-scattering approximation" (FSA) [15,18,49]. Intuitively, the three terms in the deformation (2) correspond to configurations encountered in the process of flipping the four excited Rydberg atoms that are nearest neighbors on the A sublattice into their ground state [50].

Optimization of coefficients a and b for the 6×6 size lattice with PBCs results in $a \approx 0.040$, $b \approx 0.056$. The optimization of a, b is performed by maximizing the fidelity at the first revival, $F(T)$, using the Nelder-Mead method; see Ref. [50]. The resulting fidelity time series are shown in

Fig. 1(b) where one observes a significant improvement of the revival quality from $F \approx 0.72$ for the unperturbed model to $F \approx 0.997$ for the optimal perturbation.

IV. STRUCTURE OF EIGENSTATES

The effect of optimal deformation is strongly pronounced not only in the dynamics, but also in eigenstate properties, such as entanglement entropy. Figure 1(c) compares the entanglement of each eigenstate for the clean and perturbed models. The entanglement is calculated as $S = -\mathrm{Tr}\{\rho_{\mathcal{L}} \log \rho_{\mathcal{L}}\}$, where $\rho_{\mathcal{L}} = \mathrm{Tr}_{\mathcal{R}} |\psi\rangle \langle\psi|$ is the reduced density matrix for the bipartition of the lattice into two cylindrical subsystems $\mathcal{R}, \mathcal{L}$ of size $(L/2) \times L$, where L is the linear dimension if the lattice. In both cases, the entropy for the majority of the eigenstates depends only on energy density, consistent with ETH. The unperturbed system features no significant entanglement outliers, in contrast to 1D models where a similar plot clearly revealed the special scarred eigenstates [15,49]. At the same time, the special eigenstates still can be detected by their overlap with the $|M_A\rangle$ and $|M_B\rangle$ product states [50]. By contrast, the optimally perturbed Hamiltonian displays a special band of eigenstates with much lower entropy than any other eigenstate at similar energy density, as seen in the bottom panel of Fig. 1(c). Likewise, the deformation enhances the overlap of special eigenstates with $|M_A\rangle$ and $|M_B\rangle$ product states.

The existence of a deformation that improves the special band of eigenstates suggests that potentially one may deform the 2D Hamiltonian (1) to the point where the manifold of scarred eigenstates forms an exact su(2) representation. However, while Ref. [18] provided strong numerical evidence for the existence of exact scars in 1D models by constructing a long-range quasilocal deformation, the rapidly growing Hilbert space of 2D systems precludes us from simulating longer-range deformation terms. At the same time, the existence of such a perturbation in the 2D case is nontrivial and suggests that the existence of exact scars is not related to integrability [21]. Moreover, the leading-order deformation improves the coherence so strongly that longer-range terms may be not needed on the experimentally relevant timescales.

V. SCARS IN DECORATED LATTICES

Above we considered the square lattice—the simplest 2D bipartite lattice (see Ref. [50] for the case of a honeycomb lattice). It is interesting to explore more exotic lattices, e.g., one possibility, which does not exist in 1D, are lattices where different Rydberg atoms have different number of nearest neighbors.

The simplest bipartite lattice with different connectivity can be obtained from the honeycomb lattice by adding extra Rydberg atoms to the middle of each link, see Fig. 2(a). Such a "decorated" honeycomb lattice is bipartite, where partition A consists of atoms in the middle of the edges and partition B includes atoms located at the vertices of the honeycomb lattice. We assume that there is no Rydberg blockade between sites on the same sublattice. Under such an assumption, we

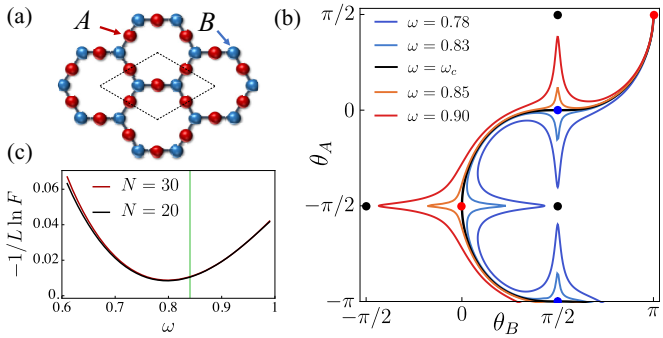

FIG. 2. (a) The decorated honeycomb lattice where each site from A (B) partition has two (three) neighbors. The unit cell contains five lattice cites. (b) Plot of the TDVP trajectories for different ω and regularization $\epsilon = 4 \times 10^{-4}$. Black points indicate the singular points, whereas red (blue) points correspond to $|M_A\rangle$ ($|M_B\rangle$) states. (c) The fidelity of the first revival of the quantum Hamiltonian with respect to the frequency ω for two different lattice sizes N. The TDVP prediction for the optimal value of ω is illustrated by the green line.

write the Hamiltonian as

$$H = \omega_A \sum_{\mathbf{r}\in A} \tilde{\sigma}^x_{\mathbf{r}} + \omega_B \sum_{\mathbf{r}\in B} \tilde{\sigma}^x_{\mathbf{r}}, \tag{4}$$

where the Hamiltonian density operator is the same as in Eq. (1), and we introduced two different Rabi frequencies (we set $\omega_B = 1$ for simplicity). We will tune ω_A below to correct for the connectivity mismatch between different sublattices. For the rest we denote $\omega_A \equiv \omega$, and use PBC. The maximally blocked states, $|M_A\rangle$ ($|M_B\rangle$) are given by exciting every site from sublattice A (B), while keeping the atoms in the other sublattice in their ground state. Now these states have an inequivalent number of excited Rydberg atoms, with the "maximally excited" state in the system being $|M_A\rangle$.

To have a quantitative understanding of dynamics, we approximate the decorated lattice by a tree with the same pattern of local connectivities using the method discussed in Ref. [17]. We project quantum dynamics on the tree onto a manifold of tensor tree states (TTSs), parametrized by two real angles $|\psi(\theta_A, \theta_B)\rangle$ using the time-dependent variational principle (TDVP) [17,50,51]. The resulting equations of motion in the TTS manifold read

$$\dot{\theta}_A = -\omega \cos^{c_A-1} \theta_B - \cos^{c_B} \theta_A \sin\theta_A \tan\theta_B, \tag{5a}$$

$$\dot{\theta}_B = -\cos^{c_B-1} \theta_A - \omega \cos^{c_A} \theta_B \sin\theta_B \tan\theta_A, \tag{5b}$$

where $c_A = 2$, $c_B = 3$ are the connectivities of sublattices A, B. For the case when $c_A = c_B$ and $\omega = 1$, Refs. [16,17] demonstrated the existence of a periodic trajectory that connects states $|M_A\rangle$ and $|M_B\rangle$ on the variational manifold.

Surprisingly, when $c_A \neq c_B$ as in the present case, the trajectory emanating from the $|M_A\rangle$ state does not reach the $|M_B\rangle$ state but instead falls into the singular point. Thus, an unstable periodic orbit does not exist for generic values of ω. In order for it to exist, it should pass through *both* $|M_A\rangle$ and $|M_B\rangle$ states. Figure 2(b) illustrates that this happens for a special value of the frequency, $\omega_c \approx 0.841$. Note that, in

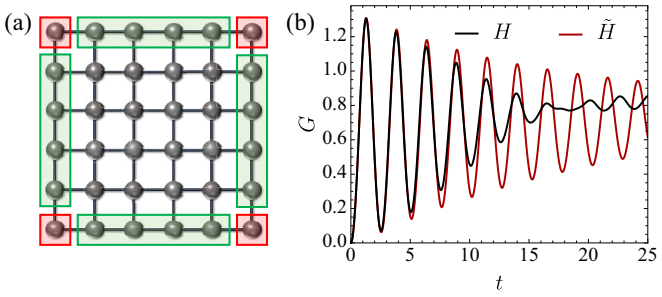

FIG. 3. (a) Illustration of the splitting of the square lattice into three different regions distinguished by the number of nearest neighbors. (b) Domain-wall dynamics for the maximally excited initial state of a 6×6 square lattice with *open* boundary conditions. The black curve corresponds to the noncorrected Hamiltonian and the red curve corresponds to the system where the corner Rabi frequency is reduced by $g_c = 0.105$.

this figure, we regularized the equations of motion by replacing $\tan\theta_A \to \tan\theta_A/(1-\epsilon\tan^2\theta_A)$ and $\tan\theta_B \to \tan\theta_B/(1-\epsilon\tan^2\theta_B)$, where the value of ϵ is small but finite. Such a regularization prevents trajectories from completely "falling" into singular points, yet we see that only at ω_c the trajectory passes through both $|M_A\rangle$ and $|M_B\rangle$ states, with the value of ω_c being independent of regularization.

Finally, we investigate the behavior of quantum fidelity at the first revival as a function of ω. Figure 2(c) shows that the fidelity has best revivals at the value of $\omega \approx 0.8$, which is close to but does not coincide with the prediction from TDVP dynamics, ω_c. The difference between the two values and also the smooth dependence of fidelity revival quality on ω may be attributed to quantum fluctuations present in the model.

The improvement of oscillations predicted by variational dynamics and confirmed in the simulation of exact quantum dynamics may be intuitively explained as enforced synchronization. Indeed, in the decorated honeycomb lattice the atoms on sublattice A experience weaker blockade due to the presence of a smaller number of nearest neighbors. Thus, the optimal fidelity revivals are achieved when the Rabi frequency ω on this sublattice is decreased compared with sublattice B. We believe that such intuition will also hold for more decorated lattices with different local connectivities c_A and c_B; see Ref. [50] for predictions for ω from FSA. On the one hand, this can open the door to the realization of scars on lattices with more exotic geometries; on the other hand, this intuition can be applied to remove the unwanted boundary effects, as we show next.

VI. BOUNDARY SYNCHRONIZATION

In experiments with Rydberg blockade, atoms are manipulated individually with optical tweezers [3,14,46,47], which enables the realization of arbitrary lattice geometries. At the same time, implementing PBCs that were used above is challenging if not unfeasible. Thus it is imperative to understand and address boundary effects. For instance, the boundary for the square lattice as large as 6×6 atoms still has more atoms compared with the "bulk" of the lattice—see Fig. 3(a). A different number of local neighbors at the boundary and in the bulk of the system leads to faster dephasing that quickly degrades fidelity revivals as well as oscillations of local observables.

Inspired by the results from decorated lattices, we propose a correction to the local Rabi frequency which depends on the local connectivity. The corrected Hamiltonian for the square lattice reads

$$\tilde{H} = H - g_C \sum_{\mathbf{r}\in\mathcal{C}} \tilde{\sigma}^x_{\mathbf{r}} - g_E \sum_{\mathbf{r}\in\mathcal{E}} \tilde{\sigma}^x_{\mathbf{r}}, \tag{6}$$

where H is the Hamiltonian from Eq. (1) and the subtracted terms include the sum over all atoms at corners ($\mathcal{C}$) which have only two nearest neighbors and those at the edges of the lattice ($\mathcal{E}$), which have three neighbors; see Fig. 3(a).

To optimize the perturbations (g_C, g_E), we maximize the fidelity on a 4×4 lattice where the full Hilbert space has dimensions $\mathrm{Dim}(\mathcal{H}) = 1234$. In this case we find an insignificant correction to the edge sites, $g_E \approx 10^{-3}$, while the corner terms acquire a much stronger correction, $g_C \approx 0.12$. Guided by this result, we completely disregard the edge correction, by setting $g_E = 0$, and focus only on the correction to the four corners of the lattice, g_C. The optimization of fidelity for the 6×6 lattice yields the optimal value $g_C \approx 0.105$ which corresponds to an approximately 10% decrease in the Rabi frequency for corners of the lattice.

We explore the effects of the perturbation on the dynamics of the experimentally observable quantity—mean domain-wall density, $G = (1/L^2)\sum_{\mathbf{r}} P_{\mathbf{r}} \sum_{\langle \mathbf{r}'\mathbf{r}\rangle} P_{\mathbf{r}'}$. Figure 3(b) compares the dynamics of the domain-wall density in the quench from $|M_A\rangle$ state for the original and boundary-synchronized Hamiltonians with open boundary conditions. While at early times the effects of the boundaries are weak (the Lieb-Robinson bound [52] suggests that boundary effects "propagate" to the bulk with a constant velocity), after four revivals the dephasing from the boundaries begins to degrade the oscillations. For the uncorrected model the domain-wall density is almost equilibrated at $t \gtrsim 15$. In contrast, the oscillations in the synchronized Hamiltonian persist for much longer times.

VII. DISCUSSION

We demonstrated the stabilization of quantum scars in 2D lattices by two complementary types of deformations of the Hamiltonian. First, we constructed a weak longer-range deformation that improves the quality of the fidelity revivals by further decoupling the scarred subspace away from the thermal bulk of the spectrum, similar to "perfect" scars in a 1D Rydberg blockade [18]. Second, inspired by the time-dependent variational-principle (TDVP) description within the TTS manifold [17], we proposed synchronization as a mechanism for improving scars on lattices of nonconstant connectivity and in the presence of boundaries. The local tuning of the Rabi frequency is feasible and can be used to experimentally mitigate the boundary effects. We expect that such a synchronization will open the door to the experimental application of scars in two dimensions akin to the π-pulse experiment in 1D [53].

An immediate question raised by our results is the interplay between the synchronization mechanism explained via TDVP and the deformation of the Hamiltonian that is explained in terms of su(2) representations. Understanding

the relation between these two mechanisms beyond the phenomenological arguments provided in Ref. [50] could provide a more complete picture and classification of possible scars. In addition, the existence of synchronization that improves scars bears a distant analogy to the collective oscillations in the BCS model [54] and collective modes in Maxwell-Bloch equation [55]. Making this analogy more quantitative could prove fruitful for generalizations of scars.

More broadly, while we demonstrated the existence of scars for several bipartite lattices; the existence of oscillations in *nonbipartite* lattices, such as triangular or kagome, remains an open question. For instance, triangular lattice features a natural partition into three sublattices and it would be interesting to explore the possibility for analogs of Z_3 scars in Rydberg chains [17,27,49]. In addition, understanding the connection between existence of scars and the ground-state phase diagram [56] and extending these results to models with longer-range blockade remains an interesting question.

Note added. Recently, Refs. [57] proposed that XXZ spin-1/2 models may acquire nonthermal eigenstates on a kagome lattice via a mechanism that utilizes geometric frustration. It remains to be understood if a similar mechanism could be useful for constrained models on nonbipartite lattices.

The data that support the figures within this paper and other findings of this study are available in Ref. [60].

ACKNOWLEDGMENTS

We acknowledge useful discussions with S. Choi, E. Demler, W. W. Ho, L. Levitov, M. Lukin and H. Pichler. A.M. and M.S. were supported by the European Research Council (ERC) under the European Union's Horizon 2020 research and innovation programme (Grant Agreement No. 850899). C.J.T. and Z.P. acknowledge support by EPSRC grants EP/R020612/1 and EP/M50807X/1. D.A.A. acknowledges support by the Swiss National Science Foundation. This work benefited from participation at KITP Follow-Up program, supported by the National Science Foundation under Grant No. NSF PHY-1748958 and from the program "Thermalization, Many body localization and Hydrodynamics" at International Centre for Theoretical Sciences (Code: ICTS/hydrodynamics2019/11).

[1] Maciej Lewenstein, Anna Sanpera, and Veronica Ahufinger, *Ultracold Atoms in Optical Lattices: Simulating Quantum Many-Body Systems* (Oxford University Press, 2012).

[2] R. Blatt and C. F. Roos, Quantum simulations with trapped ions, Nat. Phys. **8**, 277 (2012).

[3] A. Browaeys and T. Lahaye, Many-body physics with individually controlled Rydberg atoms, Nat. Phys. **16**, 132 (2020).

[4] J. M. Deutsch, Quantum statistical mechanics in a closed system, Phys. Rev. A **43**, 2046 (1991).

[5] M. Srednicki, Chaos and quantum thermalization, Phys. Rev. E **50**, 888 (1994).

[6] J. M. Deutsch, Eigenstate thermalization hypothesis, Rep. Prog. Phys. **81**, 082001 (2018).

[7] L. D'Alessio, Y. Kafri, A. Polkovnikov, and M. Rigol, From quantum chaos and eigenstate thermalization to statistical mechanics and thermodynamics, Adv. Phys. **65**, 239 (2016).

[8] H. Bethe, Zur theorie der metalle, Eur. Phys. J. A **71**, 205 (1931).

[9] L. D. Faddeev, How Algebraic Bethe ansatz works for integrable model, arXiv:hep-th/9605187.

[10] D. M. Basko, I. L. Aleiner, and B. L. Altshuler, Metal–insulator transition in a weakly interacting many-electron system with localized single-particle states, Ann. Phys. (NY) **321**, 1126 (2006).

[11] D. A. Abanin, E. Altman, I. Bloch, and M. Serbyn, Colloquium: Many-body localization, thermalization, and entanglement, Rev. Mod. Phys. **91**, 021001 (2019).

[12] W. De Roeck and F. Huveneers, Stability and instability towards delocalization in many-body localization systems, Phys. Rev. B **95**, 155129 (2017).

[13] Jae-yoon Choi, S. Hild, J. Zeiher, P. Schauß, A. Rubio-Abadal, T. Yefsah, V. Khemani, D. A. Huse, I. Bloch, and C. Gross, Exploring the many-body localization transition in two dimensions, Science **352**, 1547 (2016).

[14] H. Bernien, S. Schwartz, A. Keesling, H. Levine, A. Omran, H. Pichler, S. Choi, A. S. Zibrov, M. Endres, M. Greiner, V. Vuletic, and M. D. Lukin, Probing many-body dynamics on a 51-atom quantum simulator, Nature (London) **551**, 579 (2017).

[15] C. J. Turner, A. A. Michailidis, D. A. Abanin, M. Serbyn, and Z. Papić, Weak ergodicity breaking from quantum many-body scars, Nat. Phys. **14**, 745 (2018).

[16] W. W. Ho, S. Choi, H. Pichler, and M. D. Lukin, Periodic Orbits, Entanglement, and Quantum Many-Body Scars in Constrained Models: Matrix Product State Approach, Phys. Rev. Lett. **122**, 040603 (2019).

[17] A. A. Michailidis, C. J. Turner, Z. Papić, D. A. Abanin, and M. Serbyn, Slow Quantum Thermalization and Many-Body Revivals from Mixed Phase Space, Phys. Rev. X **10**, 011055 (2020).

[18] S. Choi, C. J. Turner, H. Pichler, W. W. Ho, A. A. Michailidis, Z. Papić, M. Serbyn, M. D. Lukin, and D. A. Abanin, Emergent SU(2) Dynamics and Perfect Quantum Many-Body Scars, Phys. Rev. Lett. **122**, 220603 (2019).

[19] K. Bull, J.-Y. Desaules, and Z. Papic, Quantum scars as embeddings of weakly "broken" Lie algebra representations, Phys. Rev. B **101**, 165139 (2020).

[20] C.-J. Lin and O. I. Motrunich, Exact Strong-ETH Violating Eigenstates in the Rydberg-Blockaded Atom Chain, Phys. Rev. Lett. **122**, 173401 (2019).

[21] V. Khemani, C. R. Laumann, and A. Chandran, Signatures of integrability in the dynamics of Rydberg-blockaded chains, Phys. Rev. B **99**, 161101(R) (2019).

[22] C.-J. Lin, A. Chandran, and O. I. Motrunich, Slow thermalization of exact quantum many-body scar states under perturbations, arXiv:1910.07669.

[23] O. Vafek, N. Regnault, and B. A. Bernevig, Entanglement of exact excited eigenstates of the Hubbard model in arbitrary dimension, SciPost Phys. **3**, 043 (2017).

[24] S. Moudgalya, N. Regnault, and B. A. Bernevig, Entanglement of exact excited states of Affleck-Kennedy-Lieb-Tasaki models: Exact results, many-body scars, and violation of the strong

eigenstate thermalization hypothesis, Phys. Rev. B **98**, 235156 (2018).

[25] M. Schecter and T. Iadecola, Weak Ergodicity Breaking and Quantum Many-Body Scars in Spin-1 XY Magnets, Phys. Rev. Lett. **123**, 147201 (2019).

[26] T. Iadecola and M. Žnidarič, Exact Localized and Ballistic Eigenstates in Disordered Chaotic Spin Ladders and the Fermi-Hubbard Model, Phys. Rev. Lett. **123**, 036403 (2019).

[27] K. Bull, I. Martin, and Z. Papić, Systematic Construction of Scarred Many-Body Dynamics in 1D Lattice Models, Phys. Rev. Lett. **123**, 030601 (2019).

[28] S. Ok, K. Choo, C. Mudry, C. Castelnovo, C. Chamon, and T. Neupert, Topological many-body scar states in dimensions one, two, and three, Phys. Rev. Research **1**, 033144 (2019).

[29] B. Mukherjee, S. Nandy, A. Sen, D. Sen, and K. Sengupta, Collapse and revival of quantum many-body scars via Floquet engineering, Phys. Rev. B **101**, 245107 (2020).

[30] A. Haldar, D. Sen, R. Moessner, and A. Das, Scars in strongly driven Floquet matter: resonance vs emergent conservation laws, arXiv:1909.04064.

[31] S. Sugiura, T. Kuwahara, and K. Saito, Many-body scar state intrinsic to periodically driven system: Rigorous results, arXiv:1911.06092.

[32] S. Chattopadhyay, H. Pichler, M. D. Lukin, and W. W. Ho, Quantum many-body scars from virtual entangled pairs, Phys. Rev. B **101**, 174308 (2020).

[33] T. Iadecola and M. Schecter, Quantum many-body scar states with emergent kinetic constraints and finite-entanglement revivals, Phys. Rev. B **101**, 024306 (2020).

[34] A. Hudomal, I. Vasic, N. Regnault, and Z. Papic, Quantum scars of bosons with correlated hopping, Commun. Phys. **3**, 99 (2020).

[35] H. Zhao, J. Vovrosh, F. Mintert, and J. Knolle, Quantum Many-Body Scars in Optical Lattices, Phys. Rev. Lett. **124**, 160604 (2020).

[36] M. Kormos, M. Collura, G. Takács, and P. Calabrese, Real-time confinement following a quantum quench to a non-integrable model, Nat. Phys. **13**, 246 (2016).

[37] A. J. A. James, R. M. Konik, and N. J. Robinson, Nonthermal States Arising from Confinement in One and Two Dimensions, Phys. Rev. Lett. **122**, 130603 (2019).

[38] N. J. Robinson, A. J. A. James, and R. M. Konik, Signatures of rare states and thermalization in a theory with confinement, Phys. Rev. B **99**, 195108 (2019).

[39] G. Magnifico, M. Dalmonte, P. Facchi, S. Pascazio, F. V. Pepe, and E. Ercolessi, Real Time Dynamics and Confinement in the $\mathbb{Z}_n$ Schwinger-Weyl lattice model for $1+1$ QED, Quantum **4**, 281 (2020).

[40] B. Buca, J. Tindall, and D. Jaksch, Non-stationary coherent quantum many-body dynamics through dissipation, Nat. Commun. **10**, 1730 (2019).

[41] J. Tindall, B. Buča, J. R. Coulthard, and D. Jaksch, Heating-Induced Long-Range η Pairing in the Hubbard Model, Phys. Rev. Lett. **123**, 030603 (2019).

[42] S. Pai and M. Pretko, Dynamical Scar States in Driven Fracton Systems, Phys. Rev. Lett. **123**, 136401 (2019).

[43] V. Khemani, M. Hermele, and R. Nandkishore, Localization from Hilbert space shattering: From theory to physical realizations, Phys. Rev. B **101**, 174204 (2020).

[44] P. Sala, T. Rakovszky, R. Verresen, M. Knap, and F. Pollmann, Ergodicity-Breaking Arising from Hilbert Space Fragmentation in Dipole-Conserving Hamiltonians, Phys. Rev. X **10**, 011047 (2020).

[45] S. Moudgalya, A. Prem, R. Nandkishore, N. Regnault, and B. A. Bernevig, Thermalization and its absence within Krylov subspaces of a constrained Hamiltonian, arXiv:1910.14048.

[46] H. Labuhn, D. Barredo, S. Ravets, S. de Léséleuc, T. Macrì, T. Lahaye, and A. Browaeys, Tunable two-dimensional arrays of single Rydberg atoms for realizing quantum Ising models, Nature (London) **534**, 667 (2016).

[47] F. Nogrette, H. Labuhn, S. Ravets, D. Barredo, L. Béguin, A. Vernier, T. Lahaye, and A. Browaeys, Single-Atom Trapping in Holographic 2D Arrays of Microtraps with Arbitrary Geometries, Phys. Rev. X **4**, 021034 (2014).

[48] R. J. Baxter, Planar lattice gases with nearest-neighbor exclusion, Ann. Comb. **3**, 191 (1999).

[49] C. J. Turner, A. A. Michailidis, D. A. Abanin, M. Serbyn, and Z. Papić, Quantum scarred eigenstates in a Rydberg atom chain: Entanglement, breakdown of thermalization, and stability to perturbations, Phys. Rev. B **98**, 155134 (2018).

[50] See Supplemental Material at http://link.aps.org/supplemental/10.1103/PhysRevResearch.2.022065 for (i) further justification of the optimal deformation/synchronization parameters, (ii) a generalization of the deformation to the honeycomb lattice, and (iii) an introduction to the tensor tree ansatz. See, also Refs. [58,59].

[51] P. Kramer and M. Saraceno, *Geometry of the Time-Dependent Variational Principle in Quantum Mechanics* (Springer, New York, 1981).

[52] E. H. Lieb and D. Robinson, The finite group velocity of quantum spin systems, Commun. Math. Phys. **28**, 251 (1972).

[53] A. Omran, H. Levine, A. Keesling, G. Semeghini, T. T. Wang, S. Ebadi, H. Bernien, A. S. Zibrov, H. Pichler, S. Choi, J. Cui, M. Rossignolo, P. Rembold, S. Montangero, T. Calarco, M. Endres, M. Greiner, V. Vuletić, and M. D. Lukin, Generation and manipulation of Schrödinger cat states in Rydberg atom arrays, Science **365**, 570 (2019).

[54] R. A. Barankov, L. S. Levitov, and B. Z. Spivak, Collective Rabi Oscillations and Solitons in a Time-Dependent BCS Pairing Problem, Phys. Rev. Lett. **93**, 160401 (2004).

[55] S. L. McCall and E. L. Hahn, Self-Induced Transparency by Pulsed Coherent Light, Phys. Rev. Lett. **18**, 908 (1967); Self-induced transparency, Phys. Rev. **183**, 457 (1969).

[56] R. Samajdar, W. W. Ho, H. Pichler, M. D. Lukin, and S. Sachdev, Complex Density Wave Orders and Quantum Phase Transitions in Square-Lattice Rydberg Atom Arrays, Phys. Rev. Lett. **124**, 103601 (2020).

[57] K. Lee, R. Melendrez, A. Pal, and H. J. Changlani, Exact three-colored quantum scars from geometric frustration, Phys. Rev. B **101**, 241111(R) (2020).

[58] W. Li, J. von Delft, and T. Xiang, Efficient simulation of infinite tree tensor network states on the Bethe lattice, Phys. Rev. B **86**, 195137 (2012).

[59] J. Haegeman, J. I. Cirac, T. J. Osborne, I. Pižorn, H. Verschelde, and F. Verstraete, Time-Dependent Variational Principle for Quantum Lattices, Phys. Rev. Lett. **107**, 070601 (2011).

[60] https://doi.org/10.26037/yareta:yaku72zyivda7mjzzbx36brora.